Split diabatic representation

B. D. Esry*
Department of Physics and J.R. Macdonald Laboratory, Kansas State University, Manhattan, Kansas 66506, USA

H. R. Sadeghpour†
ITAMP, Harvard-Smithsonian Center for Astrophysics, Cambridge, Massachusetts 02138, USA
(Received 30 June 2003; published 10 October 2003)

A split diabatic representation is proposed as a technique for generating diabatic potential curves with the maximal physical content and favorable computational characteristics. This method is a mixed adiabatic-diabatic representation, in which smoothly varying couplings appear in both the kinetic- and potential-energy matrices. It requires the solution of the first-order differential equation for the transformation matrix of the standard strict diabatic representation for which an efficient numerical scheme is also presented. A transformation propagator, akin to the Cayley-Hamiltonian time evolution operator, is employed to obtain the diabatic states while preserving unitarity. Several examples illustrate the advantages of the proposed split diabatic representation.

DOI: 10.1103/PhysRevA.68.042706 PACS number(s): 34.20.Mq, 31.50.Gh, 34.20.Gj, 31.15.Ja

I. INTRODUCTION

Nearly all systems of interest in physics do not admit separable solutions, leading to the development of many methods to find approximate solutions. One common approximation is the adiabatic approximation—holding some slow variable fixed while solving for the remaining degrees of freedom. The adiabatic approximation has been used profitably, relying on the very intuitive and physical notion of separation of time (or energy) scales. Probably the most familiar example of the adiabatic approximation is the workhorse of theoretical chemistry and molecular physics, namely the Born-Oppenheimer approximation and its variants [1].

While the Born-Oppenheimer potential curves are often used independently to generate approximate solutions, using the adiabatic eigenfunctions as basis for the fast coordinates yields *exact* solutions of the Schrödinger equation. This approach is labeled the perturbed stationary state method—or in the broader sense of adiabatic approaches, simply the adiabatic representation [2]. It requires the nonadiabatic coupling between the channels as well as the infinite set of channels. In practice, of course, the number of channels must be truncated, but numerical convergence in this respect can usually be achieved at least for slow collisions. For higher-energy collisions, the truncated basis contributes to the much-discussed electron translation factor problem [3].

Besides the need to calculate the nonadiabatic coupling in the first place, the most troublesome practical aspect of the adiabatic representation is solving the coupled radial equations themselves. Near avoided crossings of the adiabatic potential curves, the radial functions undergo rapid changes—the sharper the crossing, the more rapid the change. Numerically representing such changes is a challenging task. Moreover, it requires that the coupling near the crossings be accurately calculated, a task that is challenging in itself.

Because of these difficulties with the adiabatic representation, much effort has been invested in finding physically meaningful diabatic representations [4–6]. Generically, the adiabatic representation yields radial (slow-coordinate) equations in which the potential energy is diagonal and the coupling enters through the radial kinetic-energy operator. In contrast, the coupling in the diabatic representation resides in the potential energy, and the kinetic energy is usually diagonal. While most people agree on the definition of the adiabatic representation, definitions for diabatic representations do not enjoy similar universal agreement. This ambiguity is but one reason that—despite the difficulties mentioned above—the adiabatic representation is generally chosen over a diabatic one.

A compelling practical motivation for working in a diabatic representation, however, is the ability to cleanly eliminate physically unimportant channels from a calculation. In the adiabatic representation, eliminating the nth channel is relatively easy, but the picture that results invariably misses some essential physics because the physical configuration represented by that channel can change drastically with each avoided crossing. In contrast, diabatic states tend to track the configuration of the system, not just the nodal count as for adiabatic states. So, eliminating a single diabatic channel is equivalent to excluding a configuration of the system that has been identified as unimportant.

Another practical motivation for using diabatic representations is their slowly varying coupling elements—even in transition regions. Physically motivated diabatic potentials trace through avoided crossings just the way one would draw with a pen. More rigorously, one says that diabatic potentials are ''more physical'' when the velocity at the crossing is large or the splitting small. The diagonal kinetic energy is then the dominant part of the equation, and the crossing is traversed diabatically. In the opposite limit of small velocities, the diagonal potential of the adiabatic representation dominates, and the crossing is traversed adiabatically.

*Electronic address: esry@phys.ksu.edu; URL:http://www.phys.ksu.edu/~esry
†Electronic address: hrs@cfa.harvard.edu

Diabatic representations fall into two broad categories: those that are derived from the adiabatic representation and those that are obtained directly. Computationally, the latter are preferred since any diabatization scheme based on the adiabatic representation requires at least that the adiabatic channel functions be computed on a fine grid near the avoided crossings. Most schemes additionally require the associated nonadiabatic couplings on a similarly fine grid. On the other hand, diabatization schemes derived directly tend to have some of the advantages of the adiabatic representation itself, i.e., they are well defined and retain much of the considerable physical content of the adiabatic states. Unfortunately, there does not exist a general prescription to obtain such a physical diabatic representation.

Standard definitions of diabatic representations fail to produce physically appealing potentials if the nonadiabatic couplings do not fall off faster than R^{-1} asymptotically. Unfortunately, two of the most important examples of the adiabatic approach in scattering—the Born-Oppenheimer and the hyperspherical coordinate representations—do not satisfy this criterion.

We describe below a diabatization scheme that seeks a compromise between the various considerations listed above. While it requires first having the adiabatic representation, it yields physical diabatic channel potentials even for the hyperspherical case. Moreover, unlike some previous *ad hoc* diabatization methods in hyperspherical coordinates, this scheme, in principle, allows the radial equations to be solved exactly.

II. BACKGROUND

To put our representation into context, we will define in this section the adiabatic representation and the ''strict'' diabatic representation. We assume that there is only a single adiabatic coordinate R. While our method may generalize to several adiabatic coordinates, we prefer to preserve the simplicity of a single coordinate in order to make the logic more transparent.

The Hamiltonian for a system can in general be written as

$$H=-\frac{1}{2\mu}\frac{\partial^2}{\partial R^2}+H_{\rm ad}(R,\Omega), \tag{1}$$

where Ω represents all of the rapidly varying coordinates and R is the adiabatic parameter. The adiabatic equation is then

$$H_{\rm ad}(R,\Omega)\Phi_\nu(R;\Omega)=U_\nu^A(R)\Phi_\nu(R;\Omega). \tag{2}$$

The superscript ''A'' on the potential designates this as the adiabatic potential; the diabatic potential will be denoted with superscript ''D.'' The channel functions Φ form a complete set at every R and are used to expand the total wave function as

$$\Psi(R,\Omega)=\sum_\nu^\infty F_\nu(R)\Phi_\nu(R;\Omega) \tag{3}$$

in the adiabatic representation. With the expansion taken to infinity, the Schrödinger equation is transformed exactly to

$$\left[-\frac{1}{2\mu}\left(\mathbf{I}\frac{d}{dR}+\mathbf{P}\right)^2+\mathbf{U}^A\right]\mathbf{F}=E\mathbf{F}, \tag{4}$$

where $\mathbf{I}$ is the unit matrix, $\mathbf{U}^A$ is the diagonal matrix of adiabatic potentials, and $\mathbf{F}$ is the vector of radial channel functions. The nonadiabatic coupling matrix $\mathbf{P}$, representing the residual coupling between the fast and slow coordinates (such as the electronic and nuclear coordinates in molecules, respectively), is given by

$$P_{\lambda\nu}(R)=\langle\langle\Phi_\lambda(R)|\frac{d}{dR}|\Phi_\nu(R)\rangle\rangle.$$

In this expression, the double brackets indicate integrations over the fast coordinates only. Also, note that the matrix $\mathbf{P}$ is anti-Hermitian under interchange of the indices μ and ν. The form of Eq. (4) is reminiscent of the minimal-coupling Schrödinger equation representing a charged particle in an external field. In fact, Eq. (4) has been discussed in the language of gauge theories [4,7–9], the simplest example of which is electrodynamics.

Equation (4) can also be written as

$$\left[-\frac{1}{2\mu}\left(\mathbf{I}\frac{d^2}{dR^2}+2\mathbf{P}\frac{d}{dR}+\mathbf{Q}\right)+\mathbf{U}^A\right]\mathbf{F}=E\mathbf{F} \tag{5}$$

with the new coupling matrix $\mathbf{Q}$ defined as

$$Q_{\mu\nu}(R)=\langle\langle\Phi_\mu|\frac{d^2}{dR^2}|\Phi_\nu\rangle\rangle. \tag{6}$$

This new equation is identical to Eq. (4) through the equality

$$\mathbf{Q}=\mathbf{P}^2+\frac{d\mathbf{P}}{dR}. \tag{7}$$

When the expansion in Eq. (3) is truncated, however, Eq. (5) with $\mathbf{Q}$ obtained from Eq. (6) is more accurate since the implied sum in the $\mathbf{P}^2$ term of Eq. (7) must include the infinite set of adiabatic states to be strictly true. In the remainder of this work, we will neglect this issue with the assumptions that either our general logic can be adapted or the sum can be made to include enough states to achieve convergence for the desired elements of $\mathbf{Q}$.

The strict diabatic representation can now be defined from the unitary transformation that diagonalizes the kinetic energy in Eq. (4). This well-known transformation,

$$\frac{d}{dR}\mathbf{C}=-\mathbf{P}\mathbf{C}, \tag{8}$$

can only be unambiguously defined for a single adiabatic parameter [4]. This restriction, though, includes the important examples of the Born-Oppenheimer approximation for diatomic molecules and the adiabatic hyperspherical method. The radial equations in the strict diabatic representation are

$$\left[-\frac{1}{2\mu}\mathbf{I}\frac{d^2}{dR^2}+\mathbf{U}^D\right]\mathbf{G}=E\mathbf{G} \tag{9}$$

with the diabatic radial functions **G**,

$$\mathbf{G}=\mathbf{C}^{\dagger}\mathbf{F},$$

and diabatic potential matrix

$$\mathbf{U}^{D}=\mathbf{C}^{\dagger}\mathbf{U}^{A}\mathbf{C}.$$

The strict diabatic representation accomplishes the important goal of eliminating the sharply peaked nonadiabatic couplings, $P_{\lambda\nu}=0$, leaving only smooth off-diagonal elements in $\mathbf{U}^{D}$. Unfortunately, it also has one major drawback: due to the fact that $P_{\lambda\nu}(R\rightarrow\infty)$ do not vanish identically or vanish in a power-law fashion, the diabatic channel potentials, $\mathbf{U}^{D}_{\nu\nu}$, do not have the physical behavior we had set out to find. That is, they do not fall on top of the adiabatic potentials, tracing smoothly through avoided crossings. In particular, the tails of the diabatic potentials exhibit undesirable, unphysical behavior, and do not lead to the correct fragmentation, dissociation, or ionization limits at $R=\infty$. The culprit is the long-range coupling present in **P** for both the Born-Oppenheimer and the adiabatic hyperspherical approaches.

In the Born-Oppenheimer representation, the off-diagonal elements connecting states that have nonvanishing dipole matrix elements [4,10] approach constants with values on the order of the electronic to nuclear mass ratio as R approaches infinity. This residual coupling, related to the electron translation factor problem, leads to diabatic potentials that oscillate sinusoidally asymptotically. In fact, this constant coupling *must* be present to make up for the fact that the reduced mass is not the correct mass in the asymptotic system, where two separated atoms result. For instance, the reduced mass in the radial equation for H_2^+ is $m_p/2$, where m_p is the mass of the proton. The ground state $1s\sigma$ channel, however, correlates to $p+\mathrm{H}(1s)$ for which the reduced mass should be $m_p(m_p+1)/(2m_p+1)$. The difference is small as advertised, but nonetheless significant [11].

A two-channel example will serve to illustrate the pathological behavior of the diabatic potentials. Consider the derivative coupling matrix

$$\mathbf{P}(R)=\begin{pmatrix} 0 & P(R) \\ -P(R) & 0 \end{pmatrix}.$$

The solution of Eq. (8) for this case is

$$\mathbf{C}(R)=\begin{pmatrix} \cos\theta(R) & \sin\theta(R) \\ -\sin\theta(R) & \cos\theta(R) \end{pmatrix}, \tag{10}$$

where the rotation angle is

$$\theta(R)=\int_{R_0}^{R}P(R')dR'. \tag{11}$$

The diabatic representation thus defined coincides with the adiabatic representation at R_0, but its behavior for $R>R_0$ depends on the long-range behavior of $P(R)$. Using the transformation **C**, the diabatic potentials are thus

$$U^{D}_{11}=U^{A}_{1}\cos^2\theta+U^{A}_{2}\sin^2\theta, \tag{12}$$

$$U^{D}_{22}=U^{A}_{1}\sin^2\theta+U^{A}_{2}\cos^2\theta.$$

In the case of the Born-Oppenheimer approximation, in which the worst-case situation is $P(R\rightarrow\infty)\rightarrow\text{const}$, $\theta(R)\propto R$ and the diabatic potentials oscillate sinusoidally at large distances. Note that the magnitude of the constant asymptotic coupling only affects the period of oscillation, not its amplitude.

The situation is superficially better in the adiabatic hyperspherical approach. Here, it is the same-center, same-angular momentum, bound state to bound state off-diagonal coupling that is problematic, behaving as α/R asymptotically. While it does vanish in the limit $R\rightarrow\infty$, it nevertheless leads to diabatic potentials proportional to $\sin^2(\alpha\ln R)$ from Eqs. (11) and (12). This asymptotic mixing of the two-body channels can be traced to the fact that the hyperspherical coordinates only slowly approach the Jacobi coordinates [12]. Only for coupling that vanishes faster than R^{-1} will the asymptotic diabatic potentials take a physically sensible form.

Neither the Born-Oppenheimer nor the adiabatic hyperspherical representations, then, lead to strict diabatic potentials that have the physical asymptotic behavior we desire. Moreover, for the usual case in which the diabatic and adiabatic representations are chosen to agree at infinity, i.e., $R_0\rightarrow\infty$, the accumulated effect of these oscillations generates unphysical small-R potentials.

III. SPLIT DIABATIC REPRESENTATION

Since the root cause of the problems with the strict diabatic representation is the long-range misbehavior of the **P**-matrix elements, we propose the natural solution of splitting **P** into two parts:

$$\mathbf{P}=\mathbf{P}_{\alpha}+\mathbf{P}_{\beta}.$$

One part, say $\mathbf{P}_{\beta}$, nominally contains the long-range tail while the other, $\mathbf{P}_{\alpha}$, contains the short-range crossings. The idea is to use $\mathbf{P}_{\alpha}$ to transform away these crossings while preserving the physical long-range behavior of the adiabatic potentials by retaining $\mathbf{P}_{\beta}$ as the nonadiabatic coupling. The result is thus a mixed diabatic-adiabatic representation that hopefully retains the best features of both representations. The division of **P** among $\mathbf{P}_{\alpha}$ and $\mathbf{P}_{\beta}$ is completely arbitrary, but will affect the resulting diabatic potentials. Since all of the coupling is retained in one form or another, though, the calculation remains exact.

The split diabatic representation is defined using Eq. (8) with $\mathbf{P}_{\alpha}$ instead of the full coupling matrix **P**. Thus, we have

$$\frac{d}{dR}\mathbf{C}_{\alpha}=-\mathbf{P}_{\alpha}\mathbf{C}_{\alpha}. \tag{13}$$

For isolated crossings, $\mathbf{P}_{\alpha}$ is well approximated by a Lorentzian. As before, $\mathbf{C}_{\alpha}$ is a unitary matrix that affects the transformation from the radial functions **F** to a new set

$$\mathbf{G}_{\alpha}=C_{\alpha}^{\dagger}\mathbf{F}.$$

These new functions satisfy the radial equation

$$\left[-\frac{1}{2\mu}\left(\mathbf{I}\frac{d}{dR}+\tilde{\mathbf{P}}_\beta\right)^2+\tilde{\mathbf{U}}\right]\mathbf{G}_\alpha=E\mathbf{G}_\alpha, \tag{14}$$

where the tilde is used to denote the similarity transformation

$$\tilde{\mathbf{A}}=C_\alpha^\dagger A C_\alpha.$$

These radial equations have an intuitive form: they display the residual adiabatic behavior due to $\mathbf{P}_\beta$ and the diabatic behavior in $\tilde{\mathbf{U}}$ generated by $\mathbf{P}_\alpha$.

The diabatic channel potentials $\tilde{\mathbf{U}}_{\nu\nu}$ can now cross and will generally have the physical behavior desired for appropriate choices of $\mathbf{P}_\alpha$. Further, the channels will be coupled by both diabatic and nonadiabatic terms. The off-diagonal matrix elements of $\tilde{\mathbf{U}}$ trace smoothly through the crossings, and by construction $\mathbf{P}_\beta$ has no sharp peaks. It must still be determined whether the similarity transformation to $\tilde{\mathbf{P}}_\beta$ has reintroduced peaks from the transformation matrix $\mathbf{C}_\alpha$ itself, however.

To this end, let us again consider a two-channel problem since isolated crossings in even the most complicated problem can be profitably pictured two channels at a time. We have, then, a transformation matrix as in Eq. (10) except that the rotation angle θ is now defined from $\mathbf{P}_\alpha$, and

$$\mathbf{P}_\beta=\begin{pmatrix}0 & P_\beta(R)\\ -P_\beta(R) & 0\end{pmatrix}.$$

Note that the crossing occurs at $\theta=\pi/4$ where the channels are equally mixed; any peak due to $\mathbf{C}_\alpha$ should also occur at this point. Explicitly evaluating the transformed $\mathbf{P}_\beta$ gives

$$\tilde{\mathbf{P}}_\beta=\begin{pmatrix}0 & (\cos^2\theta-\sin^2\theta)P_\beta\\ -(\cos^2\theta-\sin^2\theta)P_\beta & 0\end{pmatrix}.$$

Thus, the similarity transformation does not reintroduce a peak in the nonadiabatic coupling at the crossing, $\theta=\pi/4$. It does, however, force the $\tilde{\mathbf{P}}_\beta$ matrix element to zero at the crossing over a distance on the order of the width of the original coupling peak profile. While this is still a rapid change, it is less problematic since $\mathbf{P}_\beta$ only includes the residual coupling which is small by construction. When more channels are included, it is likely that the off-diagonals would no longer vanish, but there should still be no peak.

IV. NUMERICAL METHOD

Traditionally, one of the impediments to using the strict diabatic approach has been the need to solve the N^2 coupled equations, Eq. (8), for $\mathbf{C}$ where N is the number of channels. By extension, the present split diabatic method will share the same drawback. We have, however, found a particularly convenient method for solving the differential equations. The essential observation is that Eqs. (8) and (13) share many properties with the time-dependent Schrödinger equation. In particular, it is a system of first-order equations whose solution obeys a unitarity condition. Simply using a straightforward Runge-Kutta integration, for instance, does not guarantee unitarity.

Many algorithms have been developed for the time-dependent problem that have the desirable property of unitary propagation. One of the more common of these is the Crank-Nicholson method [13]. As it is generally associated with the finite difference representation of the spatial coordinates with propagation in time, it will not be directly applicable here. The essence of the method—the Cayley-Hamilton form of the time evolution operator (which is itself just a Padè approximation)—can be directly applied, however.

The short-distance propagator solution of Eq. (13) is

$$\mathbf{C}(R+\Delta R)=e^{-\mathbf{P}\Delta R}\mathbf{C}(R).$$

Since $\mathbf{P}$ depends on R, this expression is not exact, but can be accurately used for small ΔR. Using $\mathbf{P}^\dagger=-\mathbf{P}$, it is easy to show that $\mathbf{C}$ remains unitary. The Cayley-Hamilton replacement is

$$e^{-\mathbf{P}\Delta R}=\frac{\mathbf{I}-\mathbf{P}\frac{\Delta R}{2}}{\mathbf{I}+\mathbf{P}\frac{\Delta R}{2}}+O(\Delta R^3),$$

which, with a little algebra, can also be shown to be unitary. A slight rearrangement gives the Crank-Nicholson-like equation for the transformation matrix propagation:

$$\left(\mathbf{I}+\mathbf{P}\frac{\Delta R}{2}\right)\mathbf{C}(R+\Delta R)=\left(\mathbf{I}-\mathbf{P}\frac{\Delta R}{2}\right)\mathbf{C}(R). \tag{15}$$

The set of N linear equations are propagated using efficient numerical routines for several right-hand sides, to obtain the transformation matrix $\mathbf{C}(R)$. It might also be possible to take advantage of the fact that the $\mathbf{P}$ matrix often has many zeros—this is especially true for $\mathbf{P}_\alpha$ in the present scheme. In practice, the step size ΔR should be chosen with an adaptive scheme for accuracy near avoided crossings. In the simplest implementation, the $\mathbf{P}$ matrix would be calculated independently, then interpolated as required for the integration above, although more elaborate schemes can easily be imagined.

V. APPLICATIONS: NUMERICAL EXAMPLES

To illustrate the split diabatic representation proposed here, we proceed with three examples in atomic and molecular collisions. The first application is to the hyperspherical potential-energy curves of the hydrogen negative ion. Next, we consider the mass-scaled antiproton-hydrogen hyperspherical potentials, and the last example is a model alkali trimer adiabatic hyperspherical potential-energy calculation.

A. H^-

In Fig. 1, we show the adiabatic hyperspherical potential curves for the excitation of the hydrogen negative ion in the $^1P^o$ symmetry [14]. The three curves shown converge to the

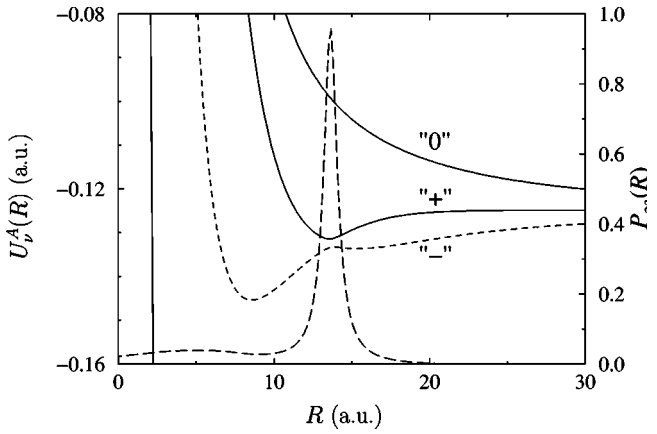

FIG. 1. Adiabatic hyperspherical potential-energy curves for H^- $^1P^o$ symmetry near the H($n=2$) threshold. The nonadiabatic coupling between the + and − curves is also shown (long dashed line). Note that it has a relatively sharp, locally Lorentzian peak at the avoided crossing.

H($2l$) threshold and can be labeled by the so-called ''near-exact'' radial quantum numbers, $A=+$, $-$, and 0, respectively [15]. The curve converging to H($1s$) is also in the figure, but the threshold is off the scale of the figure. The two + and − curves strongly repel each other near $R\approx 13$ a.u. so that the **P**-matrix element coupling them (also shown in the figure) peaks there.

Probably the simplest splitting of the **P** matrix uses only the coupling P_{23} between the + and − curves to define the diabatic transformation. The resulting diabatic potential-energy curves shown in Fig. 2 follow their adiabatic counterparts closely and cross each other at the crossing, $R\approx 13$ a.u. The + diabatic curve has a minimum near $R\approx 8.5$ a.u. and becomes repulsive after the crossing region (not shown). It supports a single resonance above the H($n=2$) threshold ($E=-0.125$ a.u.) that coincides with the celebrated H^- shape resonance [16]. By design, the curve labeled 0 and the curve converging to H($1s$) (off the scale of the graph) are identical to the adiabatic potentials since no elements coupling to these states were included in $\mathbf{P}_\alpha$. Physically, an avoided crossing signals a change in the character—shape, nodal pattern, etc.—of the channel function. The transformation to this diabatic representation thus can be thought of as preserving such properties of the channel functions.

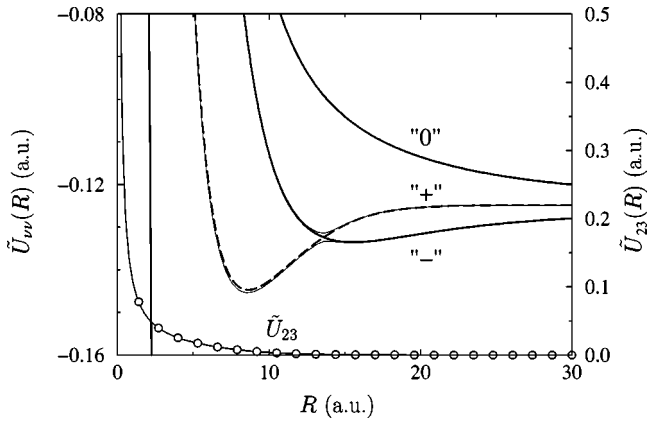

FIG. 2. Adiabatic and split diabatic hyperspherical potential-energy curves for H^- $^1P^o$ symmetry near the H($n=2$) threshold. The + diabatic curve is shown with a heavy dashed line; the − diabatic curve, with a heavy solid line. The adiabatic curves from Fig. 1 are shown as thin solid lines for comparison. The circles mark the off-diagonal diabatic coupling element between the + and − states.

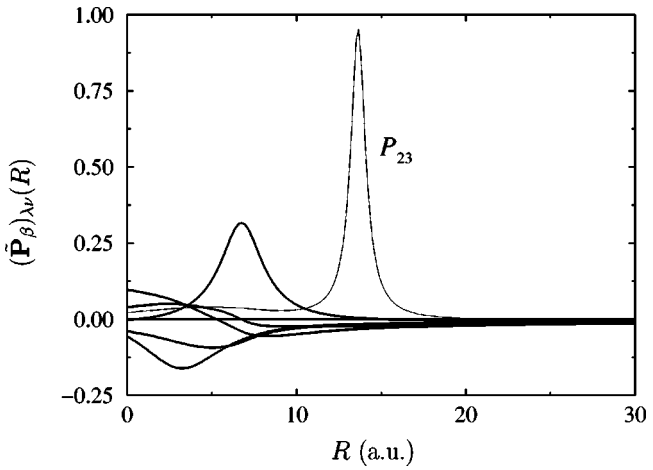

FIG. 3. The residual nonadiabatic coupling $\tilde{\mathbf{P}}_\beta$ among all of the H($n=1$) and H($n=2$) channels (heavy lines). The dashed line shows that $(\tilde{\mathbf{P}}_\beta)_{23}$ is zero (compared to the original P_{23} shown as a thin solid line).

The diabatic coupling $\tilde{U}_{23}$ is also shown in Fig. 2. This coupling is smooth and slowly varying through the crossing region as desired. All of the remaining coupling resides in the nonadiabatic term $\tilde{\mathbf{P}}_\beta$ shown in Fig. 3. Because of our selection of $\mathbf{P}_\alpha$ and $\mathbf{P}_\beta$, the original, sharply peaked nonadiabatic coupling element P_{23} is completely transformed to diabatic coupling. Thus, $(\tilde{\mathbf{P}}_\beta)_{23}$ is zero as indicated by a dashed line in Fig. 3. The + and − channels are directly coupled only by the diabatic coupling $\tilde{U}_{23}$ shown in Fig. 2. For the present purposes, the relevant point to notice about the remaining nonadiabatic coupling is that it passes smoothly through the region of the crossing of the + and − curves.

B. Mass-scaled $\bar{p}$+H

Figure 4 shows the adiabatic and diabatic hyperspherical potential curves for another Coulomb system. In this case, we examine a mass-scaled version of the $\bar{p}$+H system [17]. In this model, the masses of the p and $\bar{p}$ have been scaled to 17 times the electron mass in order to reduce the number of channels. For the realistic system, the H($1s$) threshold lies above the $p\bar{p}(n=30)$ manifold. Here, the analogous H($1s$) threshold lies instead just above the $n=3$ manifold which greatly simplifies the calculation, making it a suitable example for diabatization.

To obtain the diabatic curves in Fig. 4(b), $\mathbf{P}_\alpha$ was chosen to include only the nonadiabatic coupling between the high-

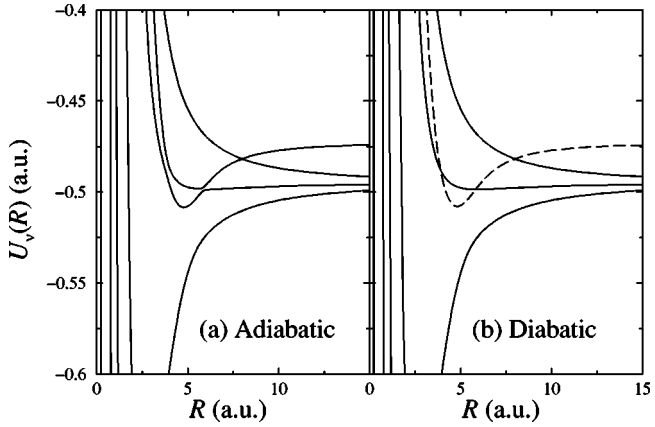

FIG. 4. The (a) adiabatic and (b) diabatic hyperspherical potential curves for a model $\bar{p}+\mathrm{H}$ system for the $J^\pi=0^+$ symmetry. The masses of the p and $\bar{p}$ have been rescaled to $\approx 17m_e$.

est three states shown in Fig. 4(a). In the pure adiabatic curves, the potential that we would like to draw correlating to the $\mathrm{H}(1s)$ threshold undergoes three avoided crossings with the upper two potentials of the $p\bar{p}(n=3)$ manifold. The transformation produces a diabatic curve that traces through these crossings, giving a physically reasonable curve representing the $\bar{p}+\mathrm{H}(1s)$ channel.

It turns out that the diabatic curves in Fig. 4(b) are not sensitive to the exact choice of $\mathbf{P}_\alpha$. For instance, the curves are identical if all of the couplings between the three curves are included or if only the nearest-neighbor couplings among these three states are included. The residual nonadiabatic couplings $\tilde{\mathbf{P}}_\beta$, however, do depend on this choice. Figure 5 shows the nonadiabatic coupling both before and after the diabatic transformation. Figure 5(a) shows the original **P**-matrix elements between the three curves in question. Note that the two nearest-neighbor couplings are extremely sharply peaked—the peak values are off the scale of the figure, ranging from 6 to 70 a.u. If only the nearest-neighbor couplings are included in $\mathbf{P}_\alpha$, the transformed nonadiabatic couplings $\tilde{\mathbf{P}}_\beta$ display sharp peaks, as shown in Fig. 5(b). The magnitude of these peaks is, however, reduced by more than an order of magnitude from the original couplings. If all the couplings between the three states are included, the residual coupling between them vanishes. In all cases, the diabatic coupling $\tilde{U}$ between the curves remains smooth and qualitatively the same as shown in Fig. 2.

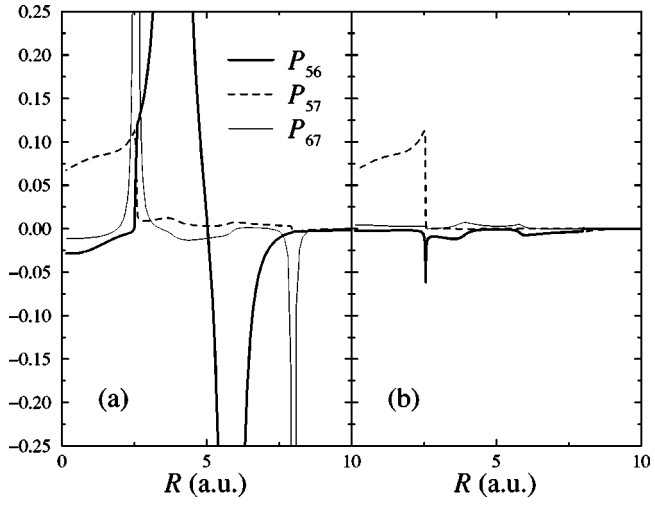

FIG. 5. The nonadiabatic coupling between the highest three states—labeled 5, 6, and 7—shown in Fig. 4. In (a), the original nonadiabatic coupling is shown, and in (b) the residual coupling $\tilde{\mathbf{P}}_\beta$ if $\mathbf{P}_\alpha$ includes only P_{56} and P_{67}.

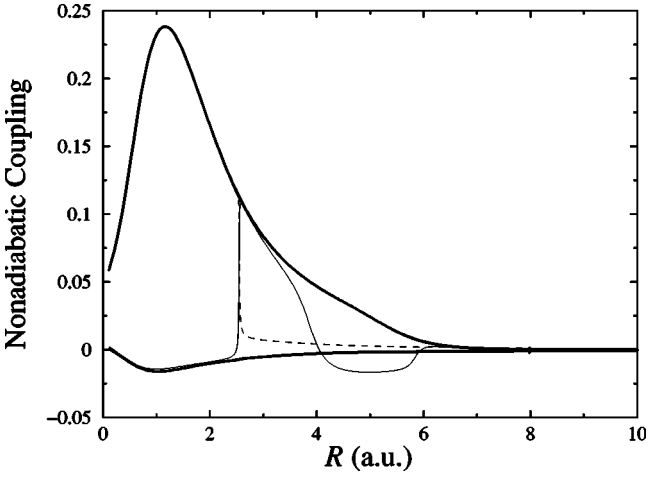

FIG. 6. The residual nonadiabatic couplings $(\tilde{\mathbf{P}}_\beta)_{17}$ and $(\tilde{\mathbf{P}}_\beta)_{16}$ (heavy lines) compared to the original nonadiabatic couplings P_{17} and P_{16} (thin lines).

In Fig. 6, we show the original nonadiabatic coupling between the $\nu=1$ channel and $\nu=6$ and $\nu=7$ (thin lines). So, even though $\nu=1$ has no sharp crossings with any state, the crossings among the higher excited channels lead to abrupt changes in the rest of the couplings as illustrated by the thin lines. The heavy lines in the figure indicate the transformed coupling $\tilde{\mathbf{P}}_\beta$. The relatively slow variation of these new couplings is a fortunate by-product of the diabatization.

It has been conjectured [17] that only the lowest $p\bar{p}$ state in each n manifold couples strongly to the $\bar{p}+\mathrm{H}(1s)$ entrance channel. With the split diabatic representation, we can more clearly test this idea by looking at the residual nonadiabatic coupling to the $\bar{p}+\mathrm{H}(1s)$ entrance channel (dashed line in Fig. 4). Figure 7 shows all of the coupling—both diabatic and nonadiabatic—with this channel ($\nu=7$). We can in fact see that the largest coupling seems to be with the lowest $p\bar{p}(3l)$ state ($\nu=4$). Furthermore, the couplings with the lowest states in the $n=1$ and $n=2$ manifolds ($\nu=1$ and $\nu=2$) are larger than the couplings with the higher $n=2$ ($\nu=3$) state. To produce this figure, we included all of the coupling between the highest three states in Fig. 4, so there is no residual nonadiabatic coupling between them. Instead, the coupling is all in the off-diagonal elements of the diabatic potential matrix. These couplings show the same trend—the energetically lower of the two channels ($\nu=5$) has a stronger coupling with the entrance channel.

C. Model Rb trimers

For our final example, we examine a model for three interacting neutral alkali-metal atoms, which has been used in

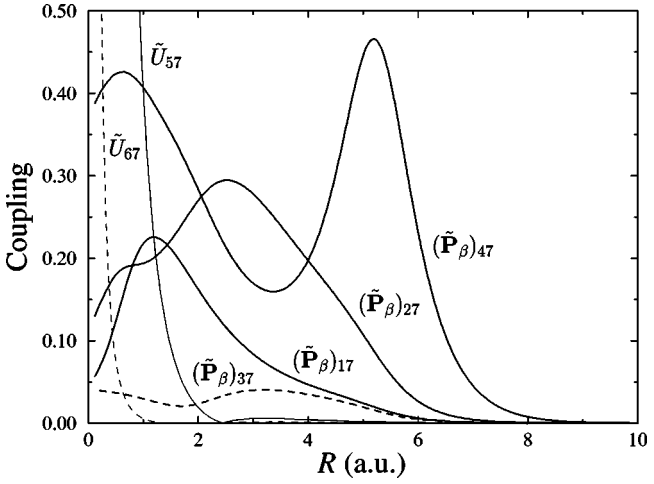

FIG. 7. The residual nonadiabatic couplings $(\tilde{\mathbf{P}}_\beta)_{17}$ and $(\tilde{\mathbf{P}}_\beta)_{16}$ (heavy lines) compared to the original nonadiabatic couplings P_{17} and P_{16} (thin lines).

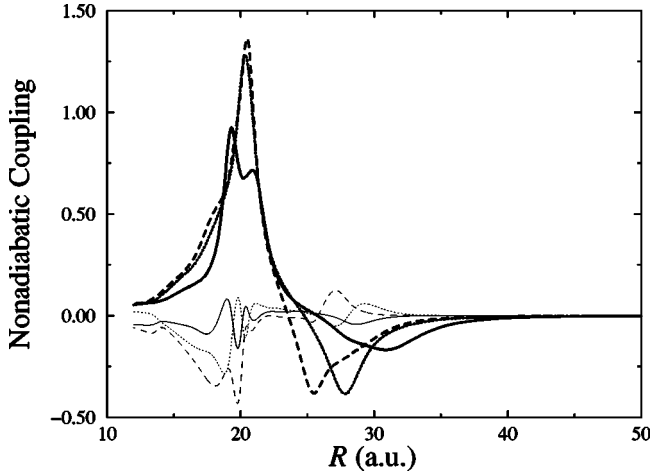

FIG. 9. The original nearest-neighbor nonadiabatic coupling (heavy lines) between the lowest four adiabatic channels. Also shown is the residual nearest-neighbor nonadiabatic coupling $\tilde{\mathbf{P}}_\beta$ (thin lines) between the lowest four diabatic channels.

the calculation of ultracold three-body recombination rates [18]. In particular, the quartet Born-Oppenheimer potential surface for three interacting Rb atoms has been approximated as a pairwise sum of realistic Rb-Rb interactions. This approximate potential was then scaled by an overall factor to reduce the number of channels to a more manageable size.

Figure 8(a) shows the lowest adiabatic hyperspherical potential curves for the case that the realistic potential is scaled by a factor of about 0.01. This neutral atom case is clearly much more complicated than the Coulomb systems considered above. There are many more broad avoided crossings as well as a few sharp ones. With only a little imagination, one can begin tracing diabatic curves through these crossings. For instance, the lowest potential shows a deep well with a small shoulder. The higher curves undergo avoided crossings that suggest the deep well could continue upwards smoothly while another diabatic potential comes down with a well sitting right on the shoulder. It has been shown that such shoulders in adiabatic hyperspherical curves correspond to changes in the geometry of the molecular system [19]. The deep well, for example, is due to nearly equilateral configurations while the shoulder represents a local energy minimum for more closely linear configurations.

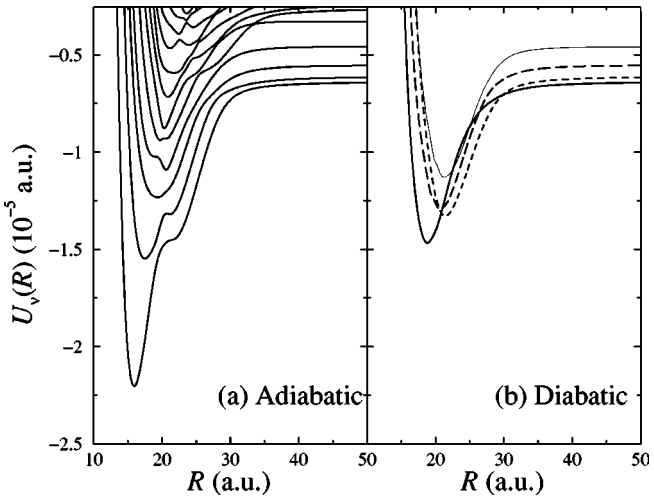

FIG. 8. The (a) adiabatic and (b) diabatic hyperspherical potential curves for a model Rb system for the $J^\pi = 0^+$ symmetry.

To generate the diabatic curves shown in Fig. 8(b), we included the nearest-neighbor coupling between the lowest 22 adiabatic channels. If only the coupling between the four lowest adiabatic channels were included, then the diabatic channels would look very different than in the figure. The structure shown began to emerge after about eight channels were included. The original nearest-neighbor nonadiabatic couplings among the four lowest channels are shown in Fig. 9 as heavy lines. These are, in fact, somewhat simpler than the couplings between higher channels. Note that they typically have larger magnitudes than the couplings in the Coulomb systems shown above as well as more complicated structure. Nevertheless, reasonable diabatic curves can be generated. In this case, however, the broad avoided crossings in the adiabatic curves lead to more mixing between the diabatic channels so that they do not as closely resemble the adiabatic potentials as before. Finally, we show in Fig. 9 the residual nonadiabatic coupling $\tilde{\mathbf{P}}_\beta$ (thin lines) between the lowest four diabatic channels. While the magnitude of the coupling has been reduced by a factor of roughly 3, the structure is as complicated as for the original coupling.

VI. SUMMARY

Curve crossings are a recurring problem in adiabatic treatments of nonseparable systems. Accurate calculations become difficult in the vicinity of such crossings, but must be carried out since essentially all inelastic processes occur at these points. Unfortunately, adiabatic solutions are generally the most straightforward to obtain and typically have substantial physical content away from the crossings. A common goal, then, is to simply ''correct'' the adiabatic potentials near the crossings. More often than not, such corrections are

applied manually rather than in a rigorous, systematically improvable manner.

We have presented a scheme to rigorously generate potential curves that coincide with the adiabatic curves away from crossings, but trace through the crossings diabatically. The resulting representation—which we label the ''split diabatic representation''—is a mixed adiabatic-diabatic representation with radial coupling in both the kinetic- and potential-energy terms. Both types of coupling, though, vary slowly with R in this representation.

We have also presented a numerical scheme to integrate the transformation equation, Eq. (8), that exactly preserves unitarity. When coupled with an adaptive step-size scheme, the method is efficient and accurate. Moreover, it can be used independently of the split diabatic scheme.

While the present method does produce diabatic potentials, it has the disadvantage of requiring the adiabatic solution and nonadiabatic couplings as input. A better scheme would take advantage of some physical insight to generate the diabatic states directly. For instance, one way to think about a diabatic state is that it follows a particular physical configuration through the evolution of the adiabatic parameter. Enforcing boundary conditions or using basis functions that represent only this configuration would generate diabatic potentials. Another way that might profitably be used to generate a diabatic state is to enforce a symmetry that is only approximately good in the full problem. In the H^- example, the $+$ and $-$ labels might be enforced somehow from the start as good quantum numbers. Once the diabatic states are found, their coupling can, of course, be calculated.

ACKNOWLEDGMENTS

This work was supported in part by a National Science Foundation grant to the Institute for Theoretical Atomic and Molecular Physics at the Harvard-Smithsonian Center for Astrophysics. B.D.E. acknowledges support from the Chemical Sciences, Geosciences, and Biosciences Division, Office of Basic Energy Sciences, Office of Science, U.S. Department of Energy.

[1] M. Born and R. Oppenheimer, Ann. Phys. (Leipzig) **84**, 457 (1927); M. Born and H. Huang, *Dynamical Theory of Crystal Lattices* (Oxford University, New York, 1954).
[2] D.R. Bates and R. McCarroll, Proc. R. Soc. London, Ser. A **245**, 175 (1958); W. Fritsch and C.D. Lin, Phys. Rep. **202**, 1 (1991).
[3] J.B. Delos, Rev. Mod. Phys. **53**, 287 (1981).
[4] T. Pacher, L.S. Cederbaum, and H. Köppel, Adv. Chem. Phys. **34**, 293 (1993), and references therein.
[5] T.G. Heil, S.E. Butler, and A. Dalgarno, Phys. Rev. A **23**, 1100 (1981).
[6] Y. Sun *et al.*, Int. Rev. Phys. Chem. **15**, 53 (1996); A.B. Alekseyev *et al.*, J. Chem. Phys. **113**, 1514 (2000).
[7] C.A. Mead and D.G. Truhlar, J. Chem. Phys. **70**, 2284 (1979).
[8] J. Moody, A. Shapere, and F. Wilczek, Phys. Rev. Lett. **56**, 893 (1986).
[9] B. Zygelman, Phys. Rev. Lett. **64**, 256 (1990).
[10] D.W. Jepsen and J.O. Hirschfelder, J. Chem. Phys. **32**, 1323 (1960).
[11] M.J. Jamieson and B. Zygelman, Phys. Rev. A **64**, 032703 (2001).
[12] J.H. Macek, Phys. Rev. A **31**, 2162 (1985).
[13] W.H. Press, S.A. Teukolsky, W.T. Vetterling, and B.P. Flannery, *Numerical Recipes, The Art of Scientific Computing*, 2nd ed. (Cambridge University Press, Cambridge, 1995).
[14] H.R. Sadeghpour, Phys. Rev. A **43**, 5821 (1991).
[15] C.D. Lin, Phys. Rep. **257**, 1 (1995), and references therein.
[16] M.E. Hamm *et al.*, Phys. Rev. Lett. **43**, 1715 (1977); H.R. Sadeghpour, C.H. Greene, and M. Cavagnero, Phys. Rev. A **45**, 1587 (1992).
[17] B.D. Esry and H.R. Sadeghpour, Phys. Rev. A **67**, 012704 (2003).
[18] B.D. Esry, J. Burke, and C.H. Greene, Phys. Rev. Lett. **83**, 1751 (1999).
[19] D. Blume and C.H. Greene, J. Chem. Phys. **113**, 4242 (2000).